The Effects of Protein Environment on the Low Temperature Electronic Spectroscopy of Cytochrome *c* and Microperoxidase-11

Eric S. Manas,* Jane M. Vanderkooi, and Kim A. Sharp

Johnson Research Foundation, Department of Biochemistry and Biophysics, University of Pennsylvania School of Medicine, Philadelphia, Pennsylvania 19104-6089

Received: March 10, 1999; In Final Form: May 17, 1999

Low temperature UV-visible spectra of cytochrome *c* and microperoxidase-11 are studied experimentally and theoretically using quantum chemical and Poisson−Boltzmann electrostatics models. Spectral splitting in the Q(0,0) visible absorption band is observed at low temperature (<180 K) in all cytochromes *c* studied. The Q-band is also found to be blue-shifted with decreasing temperature for cytochrome *c* and microperoxidase-11. Variations in the energy and splitting of the Q-band are interpreted in terms of heme distortions and interactions of the heme charge distribution with the internal electric field of the heme pocket, generated by charged and polar groups in the protein. The temperature dependence of the spectra is interpreted in terms of coupling of the heme electronic transitions to low frequency vibrational modes and thermal expansion/contraction of the protein−solvent lattice.

I. Introduction

Electronic transitions involving the porphyrin ring of heme proteins present a valuable tool for probing the heme pocket environment. This is due to the high susceptibility of the macrocycle π-electron cloud to perturbations by the surrounding protein. Such perturbations can arise from structural distortions of the porphyrin ring,[1−8] and also from the internal electric field characteristic of condensed phase systems.[9−17] Thus, the protein can modify the porphyrin electronic orbitals and energy levels, which in turn can be studied by UV−vis spectroscopy.

The visible absorption spectrum of ferrous cytochrome *c* (cyt *c*) consists of two main bands: the Q(0,0) band or α-band just above 18000 cm^{-1}, which is considered to be a purely electronic transition involving the porphyrin ring of the heme group, and the higher energy Q(0,1) band or β-band, which is considered to be composed of many heme vibronic transitions.[18] The origin of the purely electronic Q-band transition of porphyrins can be understood with the help of the 4-orbital model proposed by Gouterman.[18] Under D_{4h} symmetry, it is possible to identify two nearly degenerate electronic transitions. The first is a $\pi-\pi^*$ transition from the highest occupied molecular orbital (HOMO) of a_{1u} symmetry to the doubly degenerate lowest unoccupied molecular orbital (LUMO) of e_g symmetry. The other is a transition from the HOMO-1 orbital of a_{2u} symmetry to the e_g symmetry LUMO. Due to the accidental degeneracy of these two transitions, strong mixing between them occurs, resulting in a higher energy in-phase linear combination (giving rise to the strongly allowed Soret or B-band) and a lower energy out-of-phase linear combination (giving rise to the weakly allowed Q-band). It has been known for a long time that the Q(0,0) band of Fe(II) cyt *c* and other heme proteins shows splitting, either at room temperature, or as the temperature is lowered.[19−31] For example, the Q(0,0) band of horse heart Fe(II) cyt c shows resolved Q(0,0) splitting below 180 K.[19] The reason for this splitting is typically attributed to a reduction in molecular symmetry due to the surrounding protein. In principle, a symmetry lowering environment is capable of removing the 2-fold degeneracy of the electronic transition, resulting in a splitting of the absorption band. In practice however, the exact origin of the symmetry reduction remains unclear.

The internal electric field (inside the heme pocket) of cyt *c* and myoglobin has been measured by Stark-effect hole burning spectroscopy,[10,11] and was found to be on the order of tens of MV/cm. The values obtained are also consistent with Poisson−Boltzmann electrostatics calculations of the heme pocket field.[15] The large magnitude of these internal fields (a factor or 40 greater than the internal fields measured for *n*-alkane matrices[32,33]), has been attributed to the presence of charged and polar groups in the vicinity of the heme, such as the unprotonated heme propionates or the strong field axial ligands his18 and met80.[10,11,14,19] With such large electric fields, one might expect a significant internal Stark effect that would break the Q-band degeneracy, though it is unclear if the magnitudes of the observed spectral splittings are consistent with the magnitude and spatial dependence of the measured internal field.

It is also possible to lower the symmetry of the porphyrin ring (to a point group that does not allow for degenerate eigenstates) by distorting the ring or by asymmetrically substituting the peripheral groups. In many cases, the porphyrin ring maintains effective D_{4h} symmetry upon asymmetric peripheral substitution,[34] although the influence of the two heme propionates might better fall under the category of an electric field perturbation, since the negatively charged carboxyl groups (assuming they are unprotonated) are separated from the porphyrin ring by four bond lengths. In cyt *c*, the heme is covalently bound to the rest of the protein via thioether linkages with two cysteine residues. It has been shown, using a normal coordinate decomposition of high resolution X-ray crystallographic coordinates, that the porphyrin ring of the heme is significantly distorted from planarity and that the type of distortion is conserved across different species.[1,2,8] Thus, it is possible that this distortion leads to a removal of the degeneracy of the e_g LUMO, resulting in a splitting of the Q-band. Again

* To whom correspondence should be addressed. Phone 215-898-8783. E-mail: esm@mail.med.upenn.edu.

10.1021/jp9908552 CCC: $18.00
Published on Web 07/13/1999

however, it is unclear if the distortions observed in cyt *c* are capable of producing a splitting with the magnitudes observed experimentally.

The transition energy and lineshape of the Q-band in heme proteins has also been shown to vary with temperature.[19,35−37] The integrated Q(0,0) band intensity was shown to increase by almost a factor of two in lowering the temperature from 290 to 10 K for horse heart cyt *c*.[19] The Soret band of myoglobin and other hemeproteins also shows a spectral shift and line narrowing as the temperature is lowered, which has been interpreted in terms of quadratic electron−phonon coupling between the heme and the low-frequency vibrational modes of the protein.[35] In these studies, the line width and transition energy of the Soret band were found to be well described at low temperatures (<180 K) by coupling of the heme electronic transition to low frequency harmonic vibrations. However, deviations from harmonic behavior were indicated at higher temperatures, suggesting that the cryosolvent (e.g., glycerol−water) glass transition leads to large scale motions of the protein, characteristic of jumping between different conformational substates. This also suggests the possibility that, at low temperatures, these substates can become "frozen out", which may also have implications for any observed spectral splitting. Electron−phonon coupling has also been used to explain the temperature dependent absorption spectra of impurity crystals, and it has been shown that thermal expansion/contraction of the crystal lattice can also make a significant contribution. Since the heme distortion in cyt *c* is likely to be imposed by the cysteine linkages to the protein, it is possible that changes in this distortion with temperature also make a contribution to the temperature dependent spectral shift.

In this paper, we consider the temperature dependence of the Q-band region absorption spectra for cyt *c* from different species. This presents a set of structural homologues for which high resolution x-ray crystallographic data are available and that differ only by certain residues along the amino acid sequence. The nonconserved residues can thus lead to changes in the heme pocket environment through either electrostatic interactions (the residues can be charged or electrically neutral, and have either polar or nonpolar side chains) or by small changes in the heme structure. We also consider the model compound microperoxidase-11 (MP-11), which is a water soluble undecapeptide obtained by peptic hydrolysis of cyt *c*.[38,39] Our main goal is to elucidate the relative contributions of electrostatic interactions and porphyrin ring distortion on the Q(0,0) band splitting by studying how the splitting varies from species to species and using appropriate theoretical models. We will also use the temperature dependence of the Q-band for cyt *c* and MP-11 to clarify the nature of the coupling of the heme electronic transition to vibrations of the surrounding matrix. This will hopefully also yield information about how the overall protein conformation depends on temperature.

This paper is organized as follows. In section II, we outline the experimental methods used, and in section III, we describe our use of Poisson−Boltzmann electrostatics and quantum chemical methods to study the absorption spectrum of cyt *c*. In section IV we present the temperature dependence of the Q-band region absorption spectra for cyt *c* taken from horse heart, tuna heart, and yeast, and also for microperoxidase-11 taken from horse heart cyt *c*. In the next two sections, we analyze the low temperature Q(0,0) band for different species of cyt *c*, and we examine the relative contributions of porphyrin ring distortion and electrostatic interactions to the Q(0,0) band splitting. The studies of ring distortion utilize the ZINDO/S semiempirical method, while the studies of electrostatic effects utilize electric fields computed using Poisson−Boltzmann electrostatics, incorporated into a five-state quantum mechanical model of the porphyrin ring. In section VII, we examine how coupling between the heme electronic transitions and low-frequency vibrations can lead to the temperature dependent Q-band shifts we see for cyt *c* and MP-11. A discussion and conclusions appear in the final section.

II. Experimental Procedures

Cytochrome *c* from horse heart, tuna heart, bovine heart, chicken heart, porcine heart, and baker's yeast (Saccharomyces cerevisiae), as well as Microperoxidase-11 from horse heart, was obtained from Sigma Chemical Co. (St. Louis, MO) and used without further purification. These proteins were reduced to their Fe (II) forms by addition of dithionite after dissolving the protein. The pH was ∼6−7 for all measurements.

For all UV−vis absorption measurements, the solvent used was a 10 mM phosphate buffer diluted to 50% by volume with glycerol. The sample concentration was 1−5 mM. A Hitachi U-3000 UV−vis spectrophotometer was used to measure the spectra. The path length of sample cell was 0.05 mm and CaF_2 windows were used. The spectral resolution was 0.1 nm, and the spectra were de-convoluted using PeakFit (Jandel Scientific Software, CA). Low-temperature measurements were obtained using a top-loading OmniPlex cryostat (APD Cryogenics, Allentown, PA) with low pressure He as an exchange gas. The insulating vacuum was maintained using a TURBOVAC turbomolecular pump in conjunction with a TRIVAC rotary vane forevacuum pump and a TURBOTRONIK frequency converter obtained from Leybold Vacuum Products (Export, PA). Sapphire windows were used for the cryostat sample and vacuum ports. The temperature was controlled using a digital temperature controller (Scientific Instruments, Inc.) in conjunction with silicon diode sensor and heater placed near the sample.

III. Computational Modeling

Quantum chemical calculations on the heme group utilized the ZINDO/S semiempirical method developed and parameterized for spectroscopy by Zerner and co-workers[40−42] as implemented in the HyperChem molecular modeling software package (HyperCube, Inc., Gainesville, FL). ZINDO/S is a modification of the intermediate neglect of differential overlap (INDO) method and uses a parameterized Mataga−Nishimoto potential to calculate Coulomb integrals. Singles configuration interaction (SCI) was used in conjunction with the ZINDO/S method to calculate optical spectra. The excited states obtained from an SCI calculation consist of linear combinations of single particle excitations from the occupied orbitals of the Hartree−Fock ground state to higher energy virtual orbitals. The ground state is unperturbed by an SCI calculation, as predicted by Brillouin's theorem.[41] Analysis of the molecular charge distribution for porphyrins utilized the Gaussian 94 software package.[43]

As will be demonstrated in the following section, the absorption spectrum of Fe(II) cyt *c* is typical of low-spin hypsoporphyrins.[44] Therefore, in order to simplify our calculations, the heme group is modeled as low spin Fe(II) porphine (Fe(II)P), i.e., the peripheral groups and axial ligands are neglected in the quantum mechanical calculation and substituted with hydrogen atoms.[45,46] We found that this model gives an absorption spectrum similar to that of a closed subshell metal porphine such as ZnP, with blue shifted absorption peak positions characteristic of hypsoporphyrins.

Electrostatics calculations on the protein and surrounding solvent were performed using the software package DelPhi.[47−50] These calculations obtain finite difference solutions to the Poisson−Boltzmann equation:

$$\nabla[\epsilon(\mathbf{r})\nabla\phi(\mathbf{r})] - \kappa(\mathbf{r})^2\epsilon(\mathbf{r})\sinh[\phi(\mathbf{r})] = -4\pi\rho(\mathbf{r})/k_B T \quad (1)$$

where $\phi(\mathbf{r})$ is the electrostatic potential in units of $k_B T/e$ (k_B is the Boltzmann constant, T is the absolute temperature, and e is the elementary charge unit), $\epsilon(\mathbf{r})$ is the (position dependent) dielectric constant, $\rho(\mathbf{r})$ is the fixed charge density (in units of e), and $\kappa(\mathbf{r})$ is the Debye−Hückel constant, which is proportional to the square root of the ionic strength: $\kappa(\mathbf{r})^2 = 8\pi e^2 I/\epsilon(\mathbf{r})k_B T$. In the absence of mobile ions, $\kappa(\mathbf{r}) = 0$ everywhere and eq 1 reduces to the Poisson equation. Visualization of the electrostatic potential and fields was performed using the software package GRASP.[51]

A two-dielectric model is used for the protein−solvent system, with the dielectric boundary defined by the solvent accessible surface of the protein. PARSE values were used for the atomic radii.[52] Two types of charge assignment schemes were used. First, in order to assess the contributions of ionizable residues to the heme pocket electric field, a formal charge set was used in which charges were assigned according to the most likely protonation state of each residue at the experimental pH.[14] In this scheme, a charge of −0.5 was assigned to the OD1 and OD2 Asp oxygens, the OE1 and OE2 Glu oxygens, and also to the oxygens of the heme propionates. In addition, a charge of +0.5 was assigned to the NH1 and NH2 Arg nitrogens and +1.0 was assigned to the Lys NZ nitrogen. In the second scheme, charges were assigned to the protein residues according to the PARSE charge set[52] in order to assess the additional polar contributions to the heme pocket electric field. It is expected that these contributions will be especially important when the residue−heme distance approaches the charge separation lengths in the residue, which is when near-field effects are often large. The interior (protein) dielectric constant was assumed to be 2, which accounts for the electronic polarizability of the protein. The exterior (solvent) dielectric constant was taken to be 50 for a water/glycerol mixture, although we found that the results were not particularly sensitive to the exact value chosen. The experimental ionic strength of 0.1 M was taken in all calculations. Coordinates for cytochrome *c* were taken from the entries 1HRC.PDB,[53] 5CYT.PDB,[54] and 1YCC.PDB[55] of the Brookhaven Protein Data Bank for horse heart (HH), tuna heart (TH), and yeast (Y) cyt *c*, respectively. Hydrogens were added using the Biopolymer module of the Insight II software package (Biosym Technologies, San Diego, CA). Figure 1a shows the structure of HH cyt *c* (TH and Y cyt *c* are structural homologues). As mentioned in the introduction, MP-11 is a segment of HH cyt *c* obtained by peptic hydrolysis of the protein. The structure of this portion of HH cyt *c* is shown in Figure 1b, and consists of the sequence: val11-glu12-lys13-cys14*-ala15-glu16-cys17*-his18†-thr19-val20-glu21. The porphyrin ring is tethered to the sequence at the cys14* and cys17* residues, and Fe is axially coordinated by his18†. In cyt *c*, Fe is also coordinated by met80†.

Because of the degree of π-conjugation in the porphyrin moiety, it is likely that the electric field generated by the protein will induce a significant polarization in the heme. We note the possibility that a polarized heme can generate a significant reaction field in the protein−solvent system, and if this reaction field is large enough, it could polarize the heme further. In addition, the electronic polarization of the protein−solvent system can respond to any changes in the heme polarization during excitation.[56−58] However, as mentioned in the Introduction, previous studies have shown that the internal protein electric field in the heme pocket is very large ($\sim 10^7$ V/cm),[10,11] which is only a few orders of magnitude less than typical intramolecular electric fields (for the hydrogen atom, the characteristic field experienced by an electron is roughly $|\bar{E}| \approx e/a_o^2 = 5 \times 10^9$ V/cm, where a_o is the Bohr radius and e is the electronic charge). Thus, it seems somewhat unlikely that the additional effects of the heme reaction field will polarize the heme much further. In addition, we are currently interested in comparing the effects of different protein environments on the heme. Since the heme conformation and overall protein shape is roughly the same among different species of cytochrome *c*, it is unlikely that the heme reaction field will differ significantly among these different species. Thus for simplicity, we will neglect these effects in what follows. We plan to investigate these effects in future studies.

IV. Temperature Dependence of Fe(II) cyt *c* and MP-11 Q-Bands

The Q-band region of the UV−vis absorption spectra for HH, TH, and Y Fe(II) cyt *c* is shown as a function of temperature in Figures 2a−c, respectively. The spectrum of Fe(II) cyt *c* is typical of that of low spin hypsoporphyrins.[18] In all cases, as the temperature is lowered the Q-band gradually blue shifts and the width of the Q(0,0) transition narrows. No isosbestic points are seen in any of the spectra. At approximately 180 K, the Q(0,0) band begins to show clear signs of splitting for HH and TH cyt *c*. In what follows, the lower energy component of Q(0,0) will be denoted as Q_1 and the higher energy component will be denoted as Q_2. The splitting will be denoted by $\Delta Q_o = \epsilon_{Q_1} - \epsilon_{Q_2}$. At temperatures below 100 K, this splitting is well resolved for HH ($\Delta Q_o = 119$ cm^{-1}) and TH ($\Delta Q_o = 104$ cm^{-1}) cyt *c*, but it is not as well resolved for Y cyt *c* because the splitting approaches the bandwidth magnitude. Deconvolution of the Q(0,0) band of yeast cyt *c* gives a splitting of $\Delta Q_o \sim 80$ cm^{-1} at 10 K.

As the temperature is lowered, the Q(0,1) band also blue shifts and shows increasing structure. For horse heart and tuna heart cyt *c*, in which the Q(0,0) splitting is well resolved, the vibronic lines in the Q(0,1) band also seem to show resolved splitting at low temperature. In comparison, the vibronic lines in the Q(0,1) band of yeast cyt *c* do not show well resolved splitting.

Figure 3 shows the UV−vis absorption spectrum of Fe(II) MP-11 as a function of temperature. As was the case in cyt *c*, the Q-band blue shifts with decreasing temperature, and the bandwidths narrow. However, no signs of splitting are evident, even at the lowest temperatures. There is band asymmetry, however, and it is possible to deconvolute the Q(0,0) band into two Voigt components separated in energy by about 80 cm^{-1}. It is of interest that the Q-band of MP-11 shows no resolved splitting, even though it has been shown that the degree and type of heme distortion is similar to that of the parent horse heart cyt *c*, which shows the largest splitting of all the cyt *c*'s studied here.[59] This is in addition to the fact that the charged groups closest to the porphyrin ring (i.e., the heme propionates) are the same as those in horse heart cyt *c*.

We point out that the splitting, once resolved, is insensitive to temperature. The spectral splitting does vary from protein to protein however, and we will focus on the origin of this variation in what follows. We will defer a discussion on the origin of the temperature dependent blue shift to section VII. The spectral behavior of Fe(II) cyt *c* and Fe(II) MP-11 suggests that the surrounding protein and solvent somehow lead to the spectral

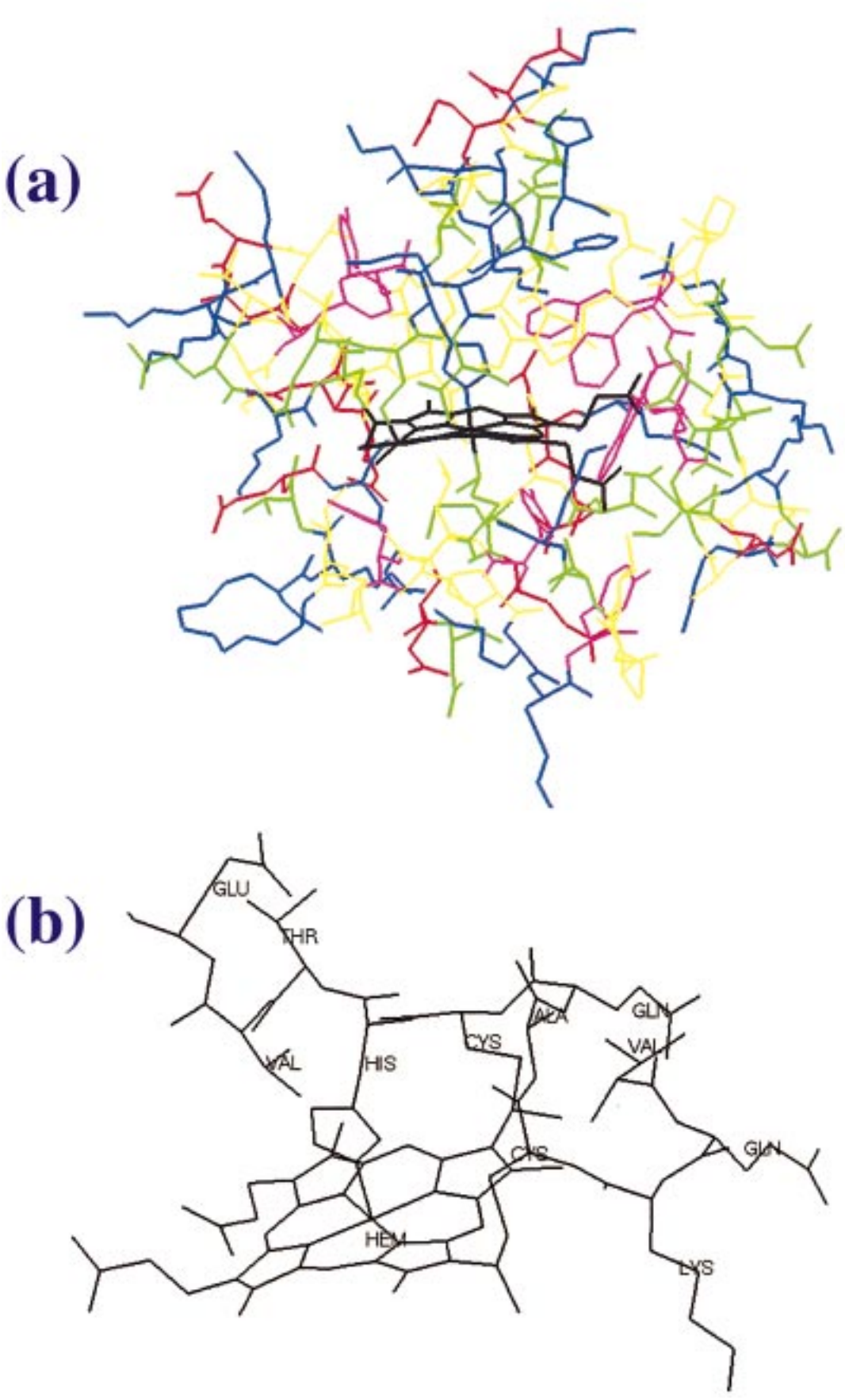

Figure 1. (a) Horse heart cytochrome *c*. The following color scheme is used for the residues according to properties of the side groups: blue-basic, red-acidic, green polar, red aromatic, and yellow hydrocarbon side group. The heme group is shown in black. (b) The segment of horse heart cytochrome *c* found in microperoxidase-11.

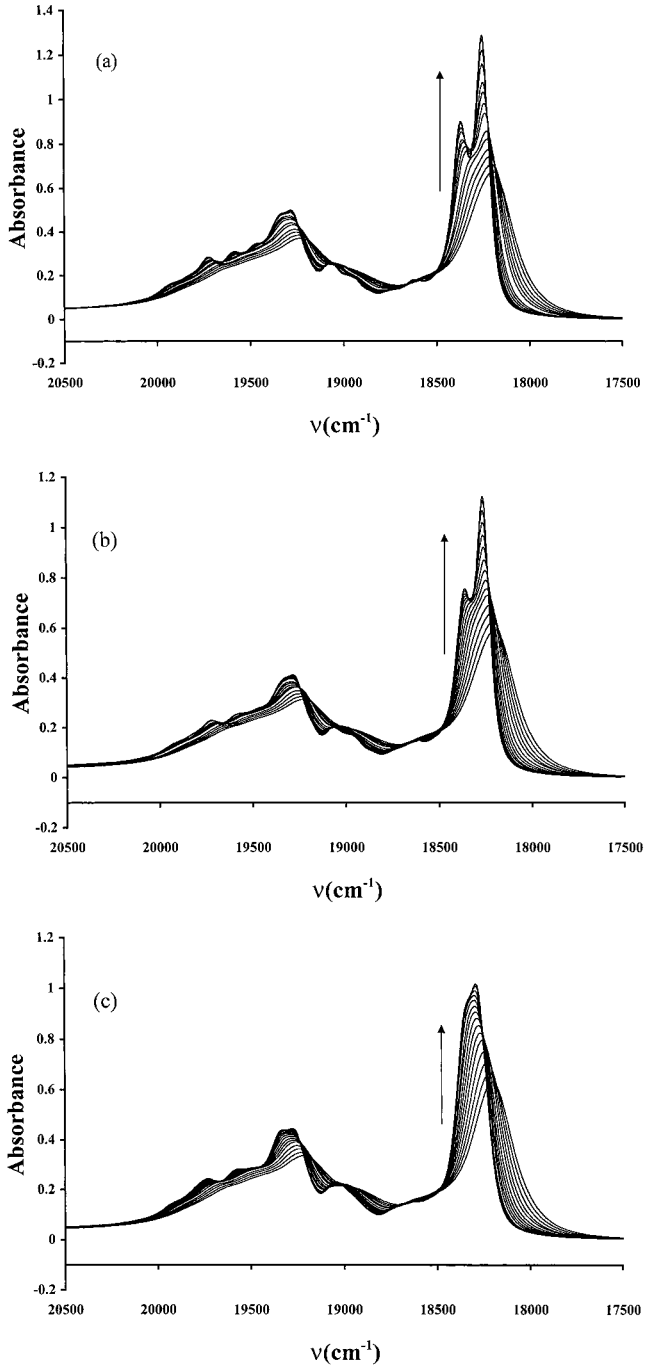

Figure 2. Q-band region absorption spectrum for (a) horse heart, (b) tuna heart, and (c) yeast cytochrome *c*, as a function of temperature. The temperature varies from 290 K to 10 K (in the direction of the arrow) in increments of 20 K. Measurements were taken as the temperature was lowered.

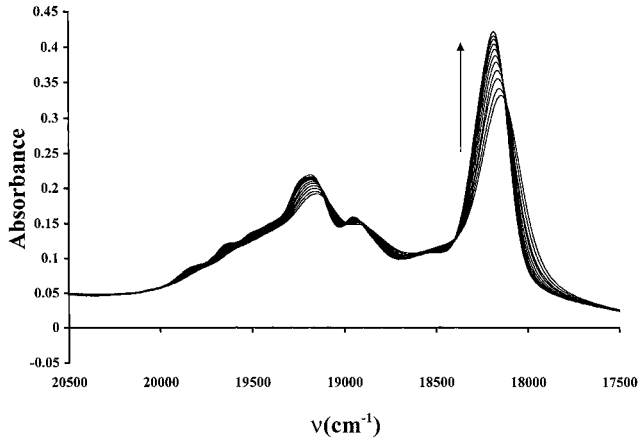

Figure 3. Q-band region absorption spectrum for microperoxidase-11 as a function of temperature. The temperature varies from 250 K to 50 K (in the direction of the arrow) in increments of 20 K. Measurements were taken as the temperature was lowered.

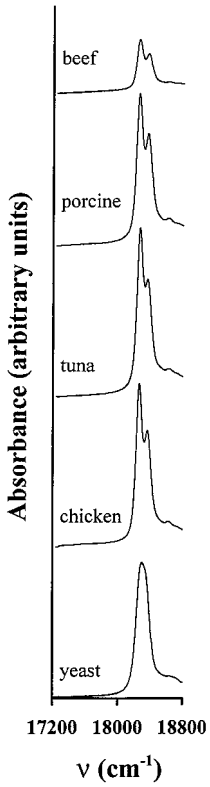

Figure 4. Q-band region absorption spectra for cytochrome *c* taken from different species, measured at 4.2 K. We point out that bovine and porcine cyt *c* have identical sequences, and the fact that they exhibit the same splitting within the resolution of the experiments serves as a verification that the splitting is uniquely determined by the protein environment.

splittings discussed above. The Q(0,0) splitting in cyt *c* has been previously attributed to a reduction from D_{4h} symmetry due to interaction with the surrounding protein.[19,21] This reduction in symmetry has also been suggested by EPR,[60] Raman,[23,61−63] and spectral hole burning experiments,[15] as well as by computational simulations.[15] As discussed in the Introduction, the general argument is that the asymmetric environment somehow removes the 2-fold degeneracy of the Q(0,0) transition, though the exact nature of the asymmetry remains unclear. In what follows, we will examine both electrostatic effects and porphyrin ring distortions as possible origins of the Q-band splitting.

V. Influence of Heme Distortion on the Q(0,0) Splitting

In order to emphasize the variation in Q(0,0) splitting among species in cyt *c*, Figure 4 shows the Q(0,0) region of the UV−vis absorption spectrum for different species of cyt *c* obtained at 4.2 K.[64] Values for the peak positions and splittings are given in Table 1.

Cyt *c* hemes typically exhibit a large ruffling distortion (B_{1u}), with minor saddling (B_{2u}) and waving (E_g) contributions, which is most likely induced via the two cysteine linkages to the protein.[2] There may also be a contribution due to hydrogen bonding between the heme propionates and various residues of

TABLE 1. Variation in Q(0,0) Band Energy and Splitting at 4.2 K among Species of Cytochrome *c*

cytochrome	ϵ_{Q_1} (cm^{-1})	ϵ_{Q_2} (cm^{-1})	ΔQ_o (cm^{-1})
yeast	18 274	18 353	80
tuna	18 267	18 371	104
chicken	18 262	18 369	107
bovine	18 257	18 372	115
porcine	18 256	18 372	116
horse	18 256	18 375	119

the protein (see Discussion). While it is clear that the various structural distortions of the heme remove the strict D_{4h} symmetry of the porphyrin ring, it is not clear whether or not these distortions can lead to Q-band splittings with the magnitudes observed for cyt *c*. In order to examine the effects of heme distortion on the Q-band, we performed ZINDO/S-SCI calculations on the Fe(II) porphyrin rings of HH, TH, and Y cyt *c*. The rings were taken from the PDB files discussed in section III, and hydrogen atoms were substituted around the periphery. The calculations yield Q(0,0) splittings ΔQ_o of 121 cm^{-1}, 45 cm^{-1}, and 578 cm^{-1} for HH, TH, and Y, respectively. The lower energy component is more intense in all cases. Although the experimental value of ΔQ_o is very well reproduced for HH cyt *c* (see Table 1), the values for TH and Y are not. We feel this may result from bond lengths in the PDB structure that differ from the equilibrium bonds lengths that would be predicted by the ZINDO method, thus resulting in a greater sensitivity to variations in bond length. However, the ZINDO results do suggest that porphyrin ring distortions from D_{4h} symmetry, in particular those distortions that occur in cyt *c* , are capable of producing Q(0,0) spectral splittings of roughly 40-600 cm^{-1}.

Further evidence suggesting that porphyrin ring distortions could lead to the splittings observed here is obtained by considering the lowest transition energy ϵ_{Q_1} for the series of proteins studied here. The data in Table 1 indicates that as ΔQ_o increases, the lowest transition energy ϵ_{Q_1} decreases. As shown in ref 8, an out of plane porphyrin distortion can energetically destabilize the electronic ground state relative to the electronic excited states. Thus, a distorted porphyrin would be expected to exhibit electronic transitions that are red shifted relative to those of its D_{4h} symmetry counterpart, in addition to splitting of electronic transitions. It is possible that an increase in distortion could simultaneously lead to an increased value of ΔQ_o with a decreased value of ϵ_{Q_1}.

We point out that the absence of any splitting in the Q(0,0) band of MP-11 may still be consistent with a significant heme distortion. Studies have shown that the distortion in MP-11 is similar to that of the parent HH cyt *c*,[59] although there is a greater degree of motional freedom. It is thus possible that as the temperature is lowered, a random distribution of many heme conformations is "frozen" in place. Therefore the greater degree of motional freedom might lead to broadening of the Q(0,0) transition, such that any splitting would be unresolved in the spectrum.

The above effects neglect the influence of the electric field due to the surrounding protein and propionate peripheral groups, and the resulting reaction field of the solvent. As mentioned earlier, the internal field of cyt *c* was measured to be quite large, and was demonstrated to have a significant effect on spectroscopic transitions involving the heme group.[10−15] However, it is unclear whether this influence can lead to the Q-band splittings observed, or contribute significantly to an already split Q-band due to heme distortion. It is to this issue that we now turn our attention.

TABLE 2. Statistics of Heme Pocket Electric Field Magnitudes and Angles for the Formal Charge Set Defined in the Text

cytochrome	horse heart	tuna heart	yeast
$\bar{E} = \sqrt{\langle E_x\rangle^2 + \langle E_y\rangle^2 + \langle E_z\rangle^2}$	14.08	13.28	15.17
$\bar{E}_{xy} = \sqrt{\langle E_x\rangle^2 + \langle E_y\rangle^2}$	13.98	12.70	15.03
σ_{E_x} = standard deviation in E_x	7.72	8.57	8.19
σ_{E_y} = standard deviation in E_y	8.65	8.55	8.64
σ_{E_z} = standard deviation in E_z	5.16	5.88	5.42
$\theta_{\bar{E}_{xy}} = \tan^{-1}[\langle E_y\rangle/\langle E_x\rangle]$	53.29	52.76	55.53
$\bar{\theta}_{E_{xy}} = \langle\tan^{-1}[E_y/E_x]\rangle$	55.59	55.04	58.24
$\sigma_{\theta_{E_{xy}}}$ = standard deviation in $\tan^{-1}[E_y/E_x]$	12.17	23.29	16.35

[a] All field magnitudes are in MV/cm, and all angles are in degrees. $\langle\rangle$ denotes averaging over all heme atoms.

VI. Electrostatic Influence on the Q(0,0) Splitting

We now consider the effects of electrostatic interactions of the porphyrin ring with the protein environment. First we will consider the effects of ionizable residues on the heme pocket electric field using the formal charge set defined in the previous section. Figure 5 shows a Grasp rendering of the electric field at the atoms of the porphyrin ring of the horse heart cyt *c* heme, computed from a Delphi potential map. Note that the field is nonuniform in magnitude, but quite uniform in direction. The field is largest in magnitude near the charged heme propionates, which make the largest contribution to the field.

Statistics of the field magnitude and angle are given in Table 2. The heme is oriented with the Fe atom at the origin and the Fe−ND bond along the *y*-axis. The average magnitude and direction are in qualitative agreement with Stark effect hole burning measurements of the internal electric field in the heme pocket.[10,11] In order to develop intuition about the effects of such a heme pocket field, it is instructive to consider a five-state model for the porphyrin ring consisting of a nondegenerate ground state $|G\rangle$ (a_{1g} symmetry), the excited states $|Q_x\rangle$ and $|Q_y\rangle$ leading to the Q (α) band, and the excited states $|B_x\rangle$ and $|B_y\rangle$ leading to the B (Soret) band (both of which have e_u symmetry). The Soret band is included in the calculation because it has a very large transition dipole moment and can play an important role in the electric field induced shift of the ground state.[10,11] When the porphyrin ring has strict D_{4h} symmetry, $|Q_x\rangle$ and $|Q_y\rangle$ (as well as $|B_x\rangle$ and $|B_y\rangle$) are doubly degenerate. However, as discussed in the previous Section, porphyrin ring distortions can remove this degeneracy (see Figure 6).

One can consider the heme pocket field to consist of a uniform field contribution and a nonuniform contribution. Alternatively, one can look at the potential energy perturbation in terms of a sum of ungerade and gerade symmetry potential functions. For example, a potential function that transforms like $x^2 + x$ (a sum of gerade and ungerade symmetry functions) will have a gradient $(2x + 1)\,\hat{\mathbf{x}}$. This gives a vector field that is uniform in direction but increases linearly in magnitude along the *x*-axis, similar to the way the electric field increases in magnitude across the porphyrin ring in Figure 5.

We first approximate the uniform contribution as a field with magnitude and direction given by the average values in Table 2. The interaction of a molecule with a uniform field **E** can be written as $\hat{V}_u = -\hat{\mu}\cdot\mathbf{E}$, where $\hat{\mu}$ is the dipole moment operator. This operator has ungerade symmetry, and will thus lead to mixing between states of opposite parity, namely, between the ground state and the Q and B excited states. For a D_{4h} symmetry

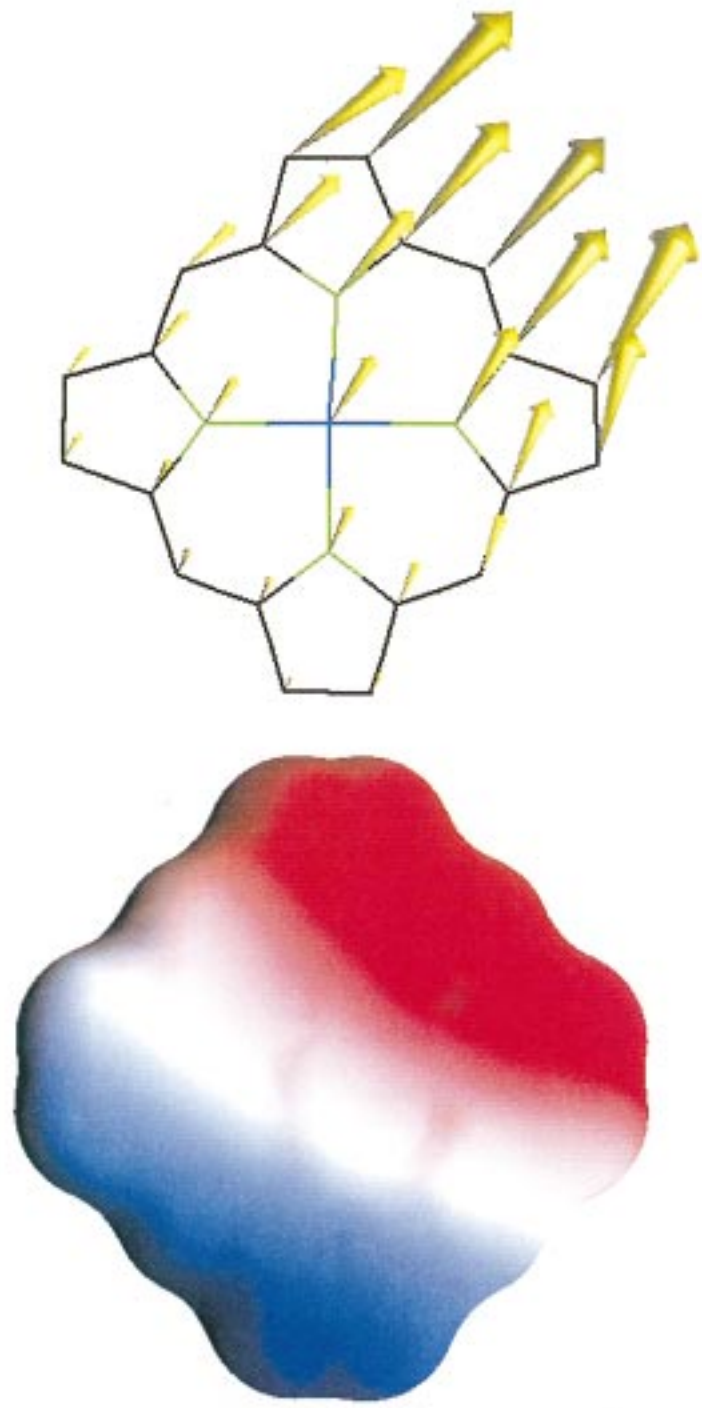

Figure 5. Grasp rendering of the electric field and electrostatic potential at the atoms of the porphyrin ring of the horse heart cytochrome *c* heme, computed from a Delphi potential map using the formal charge set discussed in the text. In this figure, the molecular surface of the porphyrin ring is color coded according to the electrostatic potential: red implies less than −500 mV and blue implies greater than +50 mV.

porphyrin, the Hamiltonian matrix can be written as

$$H = \begin{pmatrix} 0 & -\mu_{Q_x} E\cos\theta & -\mu_{Q_y} E\sin\theta & -\mu_{B_x} E\cos\theta & -\mu_{B_y} E\sin\theta \\ -\mu_{Q_x} E\cos\theta & \epsilon_{Q_x} & 0 & 0 & 0 \\ -\mu_{Q_y} E\sin\theta & 0 & \epsilon_{Q_y} & 0 & 0 \\ -\mu_{B_x} E\cos\theta & 0 & 0 & \epsilon_{B_x} & \\ -\mu_{B_y} E\sin\theta & 0 & 0 & 0 & \epsilon_{B_y} \end{pmatrix} \quad (2)$$

where $\mu_{Q_x(Q_y)}$ and $\mu_{B_x(B_y)}$ are the *x*- (*y*-) polarized Q-band and B-band transition dipole moments, $\epsilon_{Q_x(Q_y)}$ and $\epsilon_{B_x(B_y)}$ are the Q-band and B-band transition energies (*x* and *y* are degenerate in D_{4h} symmetry), and $\theta = \tan^{-1}(E_y/E_x)$ is the angle of the electric field with respect to the *x*-axis. Figure 7 shows the in-plane field dependence of the splitting ΔQ_o and the electric field induced shift of the lowest transition energy ϵ_{Q_1}. The splitting and shift are approximately quadratic in the electric field strength, as is expected for a centrosymmetric molecule in a uniform field. As can be seen in Figure 7, the main effect of such a field is to increase the transition energy. This is primarily due to the strong interaction between the ground state and

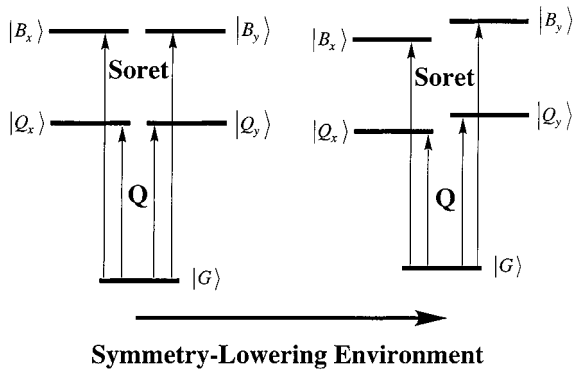

Figure 6. Schematic of the five-level model used in this work, derived from the Gouterman four-orbital model. The splitting of the $x-y$ degeneracy of the excited states due to a symmetry-lowering environment can result in a splitting of the optical transitions, as indicated.

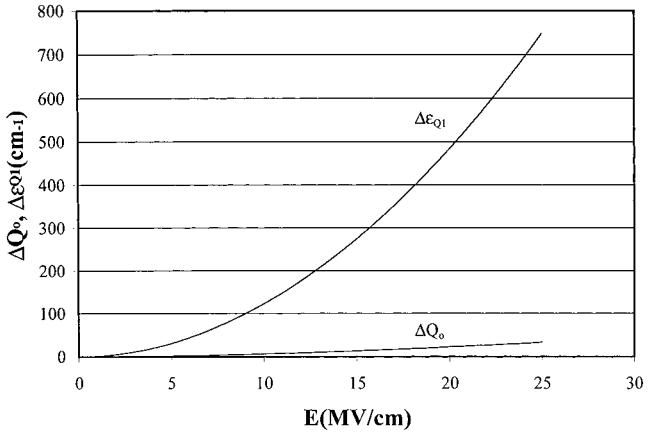

Figure 7. The in-plane field dependence of the splitting ΔQ_o and the lowest transition energy ϵ_{Q_1} for a D_{4h} symmetry porphyrin in the presence of a uniform electric field, computed by numerical diagonalization of eq 2. In this figure $\epsilon_{Q_1} = \epsilon_{Q_1} = 18000$ cm^{-1}, $\mu_{Q_{(x,y)}} = 2$ D, and $\mu_{B_{(x,y)}} = 10$ D.

B-band excited state, resulting from the large transition moment for the B-band (~10 D). The splitting of the Q-band in this model is less than 30 cm^{-1} for even the largest fields shown in Figure 7. This splitting would be too small to be resolved given the low-temperature linewidths shown in Figures 2 and 3 (the Q_1 and Q_2 line widths for cyt c are between 80 cm^{-1} and 120 cm^{-1} after deconvolution).

The origin of the Q-band splitting in this simple Stark effect model can be explained as follows. Neglecting the mixing of $|B_x\rangle$ and $|B_y\rangle$ with $|G\rangle$, the ground and Q-band eigenstates of the Hamiltonian in eq 2 are given by

$$|0\rangle = c_2\,|G\rangle - c_1|Q+\rangle \tag{3a}$$

$$|1\rangle = c_2\,|Q-\rangle = \sin\theta\,|Q_x\rangle - \cos\theta\,|Q_y\rangle \tag{3b}$$

$$|2\rangle = c_1\,|Q+\rangle + c_2|G\rangle \tag{3c}$$

where

$$|Q+\rangle = \cos\theta\,|Q_x\rangle + \sin\theta\,|Q_y\rangle \tag{3d}$$

with the $|0\rangle \rightarrow |2\rangle$ transition polarized along **E** and the $|0\rangle \rightarrow |1\rangle$ polarized orthogonal to **E** (the mixing of $|B_x\rangle$ and $|B_y\rangle$ with $|G\rangle$ will not change these polarizations). The uniform field thus results in an interaction between the states $|G\rangle$ and $|Q+\rangle$, forming the in- and out-of-phase states $|2\rangle$ and $|0\rangle$. The state $|1\rangle = |Q-\rangle$ is insensitive to the field magnitude, so $|2\rangle$ is shifted

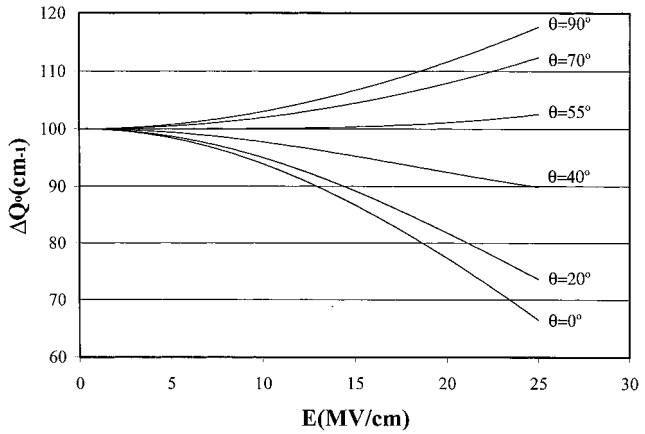

Figure 8. The splitting ΔQ_o as a function of electric field strength for a reduced-symmetry porphyrin, for different angles between the electric field vector and the *x*-polarized transition dipole moment μ_{Q_x}, computed by numerical diagonalization of eq 2. In this figure $\epsilon_{Q_1} - \epsilon_{Q_1} = 100$ cm^{-1}, with $\epsilon_{Q_1} = 18000$ cm^{-1}, $\mu_{Q_x} = \mu_{Q_y}/0.7 = 2$ D, and $\mu_{B_x} = \mu_{B_y}/0.7 = 10$ D.

relative to $|1\rangle$, and the Q-band $|0\rangle \rightarrow |1\rangle$ and $|0\rangle \rightarrow |2\rangle$ transitions are split. The magnitude of this splitting is given by $\Delta Q_o = \sqrt{(\epsilon_Q/2)^2+(\mu_Q E)^2} - (\epsilon_Q/2) \approx (\mu_Q E)^2/\epsilon_Q \approx 0.0623E^2$ cm^{-1} for $\mu_Q = 2$D, $\epsilon_Q = 18000$ cm^{-1}, and E in units of MV/cm. Thus, since the Q-band transition dipole is so small with an optical transition energy, seemingly large electric fields do not lead to significant splittings. For the same parameter set as above and $E = 13$ MV/cm for cyt *c*, the interaction $\mu_Q E = 335$ cm^{-1}, which is quite small compared to ϵ_Q, leading to a splitting of only about 10 cm^{-1} (see Figure 7).

If the Q-band is already split due to a distortion of the heme, we note that the additional effect of a uniform electric field with a similar magnitude to those found in Table 2 could either increase or decrease the Q-band splitting. This effect is shown in Figure 8, which shows the Q-band splitting as a function of electric field strength, for different angles between the electric field vector and the *x*-polarized transition dipole μ_{Q_x}. The ~*x*-polarized transition is assumed to be lower in energy. The effects observed in Figure 8 can be explained as follows. When the field is aligned along μ_{Q_x}, it induces an interaction between $|G\rangle$ and $|Q_x\rangle$, shifting $|Q_x\rangle$ closer to $|Q_y\rangle$, which remains unshifted. Thus the splitting decreases. On the other hand, when the field is along μ_{Q_y}, the resulting interaction between $|G\rangle$ and $|Q_y\rangle$ shifts $|Q_y\rangle$ away from $|Q_x\rangle$, increasing the splitting. At some intermediate angle, the shifts of both $|Q_x\rangle$ and $|Q_y\rangle$ are the same, and the field has no effect on the splitting. This angle can be estimated using second order perturbation theory: the field contribution to the splitting will be zero when the field induced shift of $|Q_x\rangle$, given by $\mu_{Q_x}^2 E^2 \sin^2\theta/\epsilon_{Q_x}$ equals the field induced shift of $|Q_y\rangle$, given by $\mu_{Q_y}^2 E^2 \sin^2\theta/\epsilon_{Q_y}$, yielding $\tan\theta = (\mu_{Q_x}/\mu_{Q_y})\sqrt{\epsilon_{Q_y}/\epsilon_{Q_x}}$. Using $\mu_{Q_x}/\mu_{Q_y} = 1.4$ yields approximately 55°. For other angles and for the field magnitudes given in Table 2, the electric field leads to a change in ΔQ_o of ±10 cm^{-1} at most. Thus, it is reasonable to expect that the uniform field contribution from the protein charged groups, primarily the heme propionates, has a negligible effect on ΔQ_o.

Before we examine the nonuniform field contribution to ΔQ_o, we will first assess the polar contributions to the heme pocket electric field. The propionate charges are omitted from the calculation for now, since their contribution was studied above. Figure 9 shows a Grasp rendering of the electric field and

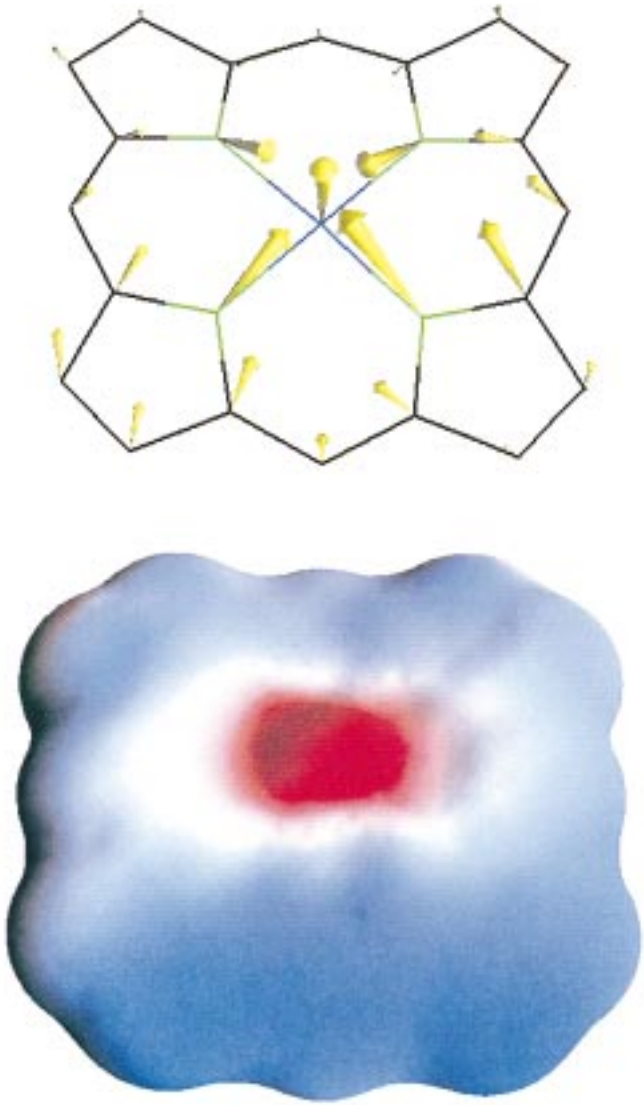

Figure 9. Grasp rendering of the electric field and electrostatic potential at the atoms of the porphyrin ring of the horse heart cytochrome *c* heme, computed from a Delphi potential map using the PARSE charge set. In this figure, the molecular surface of the porphyrin ring is color coded according to the electrostatic potential: red implies less than −1.2 V and blue implies greater than +1.2 V.

electrostatic potential for the porphyrin ring of the horse heart cyt *c* heme, computed from a Delphi potential map using the PARSE charge set. Note that the field is now nonuniform in both magnitude and direction, and the electrostatic potential is nearly centrosymmetric (gerade symmetry) with respect to the heme Fe. A detailed analysis indicates that a major contribution to the field is due to the dipole moments of the his18† and met80† residues, which are axially coordinated to the porphyrin Fe atom. Since the heme propionate charges were not included in the calculation, the field at the Fe atom is almost exactly perpendicular to the heme plane. When the propionates are charged, this "tips" the electric field vector towards these groups, but the largest component remains perpendicular to the heme plane. The electric field gradients for HH, TH, and Y cyt *c* (with the heme propionates charged) are given in Table 3.

The PARSE charges for the his18† dipole C−N−C and the met80† dipole C−S−C are very similar[65] (the difference between these dipoles leads to the small *z*-component field shown in Figure 9), so the influence on the heme electronic structure can be approximated as a perturbation with gerade symmetry. In fact, it is quite clear from Figure 9 that the electrostatic potential function has approximate gerade symmetry with respect to the heme. Thus, the effects of the nonuniform field due to the near field of the two axial dipoles, as well as the effects of the nonuniform field due to the charged heme propionates, can be treated together as a perturbation with gerade symmetry. We note that in ref 29, the axial ligation of two pyridines to Fe porphine, with the ligand planes oriented along a line through the center of the porphyrin ring and two opposite pyrrole nitrogens, was similarly treated as a perturbation that transforms like a linear combination of the A_{1g} and B_{1g} irreducible representations in the D_{4h} point group.

TABLE 3: Approximate Electric Field Gradients (MV/cm/Å) at the Heme Center Using the PARSE Charge Set with the Heme Propionates Charged

cytochrome	horse heart	tuna heart	yeast
$\partial E_x/\partial x$	−19.53	−18.26	−15.36
$\partial E_y/\partial y$	−18.35	−17.22	−15.94
$\partial E_x/\partial y$	1.18	0.61	−1.32

[a] Gradients are calculated by taking the difference between electric field components computed at opposite nitrogens, and then dividing this difference by the distance between the nitrogens.

Again we consider an initially D_{4h} symmetry porphyrin. Utilizing a multipolar expansion for the porphyrin charge distribution and truncating at the quadrupole term, the Hamiltonian matrix elements between states $|n\rangle$ and $|m\rangle$ can be approximated as

$$H_{nm} = \delta_{nm}\epsilon_n - e\sum_{i=1}^{3}\langle n|q_i|m\rangle E_i - \frac{e}{2}\sum_{i,j=1}^{3}\langle n|q_iq_j|m\rangle\frac{\partial E_i}{\partial q_j} \quad (4)$$

where q_i represents the Cartesian coordinates x, y, and z for $i =$ 1, 2, and 3, respectively. The first term in eq 4 represents the zero-field transition energies of the porphyrin ring, while the second term gives the interaction of the molecular (transition) dipoles with an electric field. Since we already showed this term to have a small effect on the Q-band splitting, we will neglect its contribution for now. The third term represents the interaction of the quadrupole moment of the molecular charge distribution with an electric field gradient. This contribution to the potential energy involves matrix elements of x^2, y^2, z^2, xy, xz, and yz and thus has gerade symmetry. Such an interaction will tend to mix states of the same symmetry. This includes mixing of the Q and B excited states with each other (off-diagonal interactions), as well as diagonal interactions representing the interaction of the field gradient with the permanent quadrupole moments of the ground and excited states.

The most direct way in which the quadrupole energy term can lead to a splitting of the Q-band is via the diagonal interactions (i.e., $n = m$ in eq 4). Although the porphyrin ring has no permanent dipole moment in any state due to the center of inversion, the states all have large permanent quadrupole moments. Performing a RHF/3-21G ab-initio calculation gives permanent quadrupole moment tensor components (diagonal matrix elements of x^2, y^2, and z^2) on the order of 100 D Å (for comparison, the permanent quadrupole strength of CO_2 is 2.3 D Å [66]). The matrix elements of xy, xz, and yz are much smaller. Neglecting these matrix elements and any off-diagonal mixing, ΔQ_o is given by

$$\Delta Q_o \approx -\frac{e}{2}\left\{\frac{\partial E_x}{\partial x}(\langle Q_y|x^2|Q_y\rangle - \langle Q_x|x^2|Q_x\rangle) + \frac{\partial E_y}{\partial y}(\langle Q_y|y^2|Q_y\rangle - \langle Q_x|y^2|Q_x\rangle)\right\} \quad (5a)$$

$$= \frac{e}{2}\left\{\frac{\partial E_x}{\partial x} - \frac{\partial E_y}{\partial y}\right\}(\langle Q_x|x^2 - y^2|Q_x\rangle) \quad (5b)$$

Equation 5 was obtained by taking the difference of the Q-state diagonal energy terms in eq 4. Equation 5a utilizes the fact that mixed derivatives like $\partial E_x/\partial y$ are small for the porphyrin ring in the heme pocket (see Table 3) and also that the matrix elements of z^2 do not differ for $|Q_x\rangle$ and $|Q_y\rangle$. Furthermore, the final equality in eq 5b assumes that the basis states $|Q_x\rangle$ and $|Q_y\rangle$ are related by a simple 90° rotation about the z-axis. Equation 5 shows that if the gradients of E_x and E_y (in the x- and y-directions, respectively) differ, *and* if the excited state charge density exhibits an "alignment" along the x- or y-axes (such that $\langle Q_x|x^2 - y^2|Q_x\rangle$ is nonzero, for instance), then ΔQ_o will be nonzero. Generally, since $|Q_x\rangle$ transforms like e_u and $x^2 - y^2$ transforms like b_{1g} in the D_{4h} point group, $\langle Q_x|x^2 - y^2|Q_x\rangle$ will transform like $e_u \otimes e_u \otimes b_{1g}$, which contains the totally symmetric irreducible representation a_{1g} and can thus be nonzero. Figure 10a shows ΔQ_o as a function of $e\langle Q_x|x^2 - y^2|Q_x\rangle$, using the electric field gradients given in Table 3 for HH, TH, and Y cyt *c*. As can be clearly seen, the trend $\Delta Q_{o,HH} > \Delta Q_{o,TH} > \Delta Q_{o,Y}$ is well reproduced, since the difference between $\partial E_x/\partial x$ and $\partial E_y/\partial y$ increases along this series (Table 3).

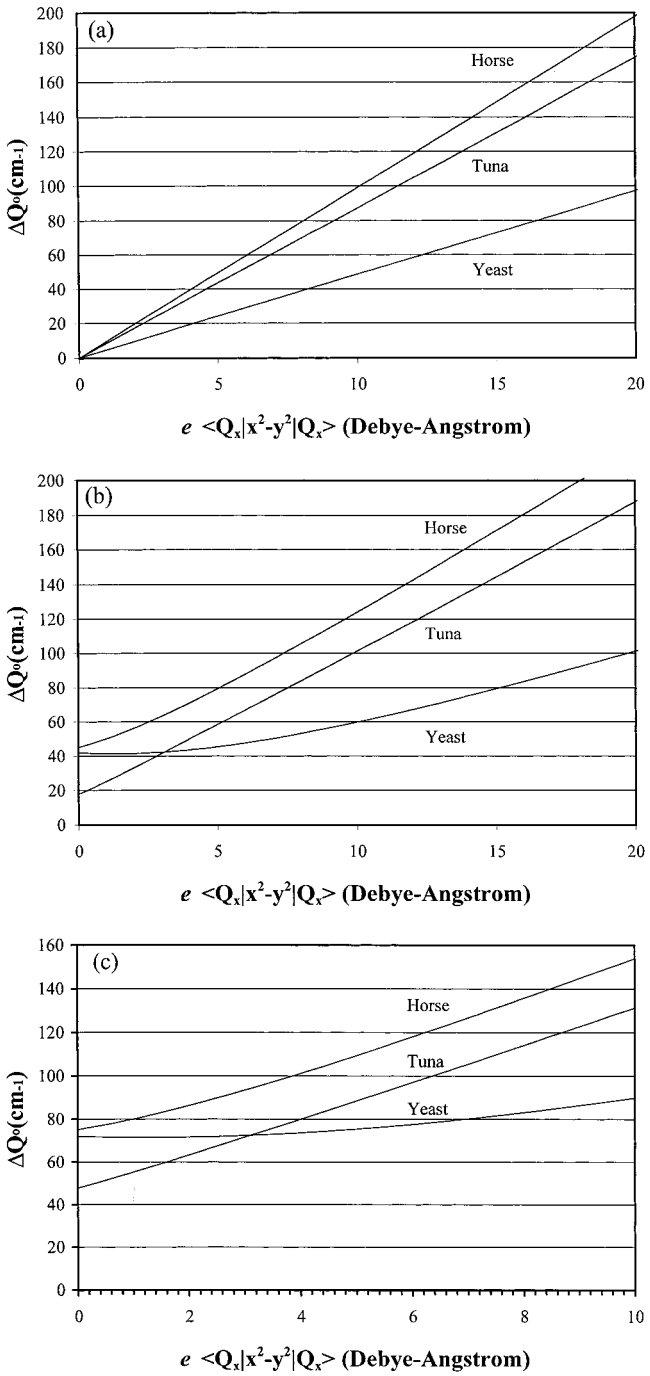

Figure 10. The splitting ΔQ_o as a function of $e\langle Q_x|x^2 - y^2|Q_x\rangle$, computed by numerical diagonalization of eq 4, for (a) a D_{4h} symmetry porphyrin, with interactions between the electric field gradients and the permanent electric quadrupole moments of the molecular eigenstates taken into account, (b) same as (a), with the additional effects of off-diagonal quadrupole matrix elements taken into account, and (c) same as (b), with the additional effects of a porphyrin ring distortion taken into account, leading to a splitting contribution of $\Delta Q_{Distortion} = 30\ cm^{-1}$. The transition dipole moments and energies are the same as those in Figure 6.

Figure 10b shows a set of curves that are similar to those in Figure 10a, but with the uniform field contribution (with the electric field taken from Table 2) , as well as the other off-diagonal contributions included. In this figure, we estimated the quadrupole matrix elements $e\langle n|q_iq_j|m\rangle$ between excited states

as follows. Assuming the eigenstates $|l\rangle$ of the porphyrin ring form a complete set, we can use the closure relation $\sum_l |l\rangle\langle l|$ to obtain $e\langle n|q_i q_j|m\rangle = e\sum_l \langle n|q_i|l\rangle\langle l|q_j|m\rangle$. The major contribution to the summation is then taken to be from $|l\rangle = |G\rangle$, yielding $e\langle n|q_i q_j|m\rangle \approx \mu_n\mu_m/e$ (μ_n is the transition dipole moment between the ground state and $|n\rangle$). These quadrupole matrix elements are small compared to the permanent quadrupole moments of the porphyrin ring. For instance, using $\mu_Q = 2-3$ D and $\mu_B = 10-15$ D yields $\langle Q_{(x,y)}|q_i q_j|B_{(x,y)}\rangle \approx 4-9$ D Å. Thus, the influence on the splitting is less, and the trend in ΔQ_o is reproduced for $e\ \langle Q_x|x^2 - y^2|Q_x\rangle > 3$ D Å.

We point out that the nonuniform field contribution to ΔQ_o could also reproduce the trend $\Delta Q_{o,HH} > \Delta Q_{o,TH} > \Delta Q_{o,Y}$ if the Q-band is already split by a constant amount due to distortion of the porphyrin ring. Using the same assumptions that lead to eq 5b, we obtain an estimate of the non-uniform field contribution to the Q-band splitting for a distorted porphyrin

$$\Delta Q_o \approx \Delta Q_{\text{Distortion}} + \frac{e}{2}\left\{\frac{\partial E_x}{\partial x} - \frac{\partial E_y}{\partial y}\right\}(\langle Q_x|x^2|Q_x\rangle - \langle Q_y|x^2|Q_y\rangle) \quad (6)$$

The above equation indicates that ΔQ_o still increases with the difference $\partial E_x/\partial x - \partial E_y/\partial y$ when the Q-band is split due to distortion. Figure 10c shows ΔQ_o as a function of $e\langle Q_x|x^2 - y^2|Q_x\rangle$, this time including the uniform field and off-diagonal interactions, with $\Delta Q_{\text{Distortion}} = 30\ \text{cm}^{-1}$. As in Figure 10b, the trend $\Delta Q_{o,HH} > \Delta Q_{o,TH} > \Delta Q_{o,Y}$ is reproduced for $e\langle Q_x|x^2 - y^2|Q_x\rangle > 3$ D Å. We find that $\Delta Q_{\text{Distortion}} \approx 30\ \text{cm}^{-1}$ and $e\langle Q_x|x^2 - y^2|Q_x\rangle \approx 6.6$ D Å best reproduces the observed splittings for HH, TH, and Y cyt *c*, yielding calculated splitting values of $\Delta Q_{o,HH} = 123\ \text{cm}^{-1}$, $\Delta Q_{o,TH} = 102\ \text{cm}^{-1}$, and $\Delta Q_{o,Y} = 79\ \text{cm}^{-1}$. We emphasize that these values were obtained without optimizing molecular parameters, such as the zero-field transition energies or transition dipole moments. Thus, the above calculation should not be taken as a measure of the variable parameters $\Delta Q_{\text{Distortion}}$ or $e\ \langle Q_x|x^2 - y^2|Q_x\rangle$. However, the ability of this calculation to reproduce the observed trend in ΔQ_o does serve to highlight the importance of the nonuniformity of the heme pocket internal field in determining the Q-band splitting.

VII. Temperature Dependence of the Q-Band Energy

We now discuss the origin of the temperature dependent shift of the Q-band. It has been demonstrated[35-37] that temperature shifts and broadening observed for the Soret band of myoglobin and hemoglobin can be attributed to coupling of heme electronic transitions with low-frequency vibrational modes of the surrounding matrix. As was pointed out in ref 35, the integrated intensity of weak bands like the Q-band of heme proteins is expected to depend significantly on temperature. We therefore make no attempt here to model the variation of the overall lineshape with temperature, for lack of an appropriate model to predict Q-band intensities. However, a simple model that includes quadratic electron-phonon coupling can be used to gain insight into the origin of the temperature dependent shift that we observe for cyt *c* and MP-11. The mechanism can be described as follows. For a molecule embedded in a matrix (e.g., protein−solvent matrix), when the molecule undergoes an electronic transition, the transition is coupled to the low frequency vibrations of the surrounding matrix. Thus, an optical transition can be described as a transition from a molecule in its ground electronic state with some number of matrix vibrational quanta (phonons), to a molecule in its excited electronic state with some (possibly different) number of phonons. If the electronic transition were uncoupled to the matrix phonons or only coupled to first order with respect to the normal coordinate displacements of the matrix, then the lattice vibrational frequencies would be the same whether the molecule was in the ground or excited electronic state. However, second-order electron−phonon coupling leads to a change in the phonon frequencies upon excitation of the molecule. Since the population of phonon modes depends on temperature, as given by given by the Bose−Einstein distribution $\bar{n}_k = (e^{\hbar\omega_k/k_B T} - 1)^{-1} = [\coth(\hbar\omega_k/2k_B T) - 1]/2$ (ω_k is the frequency of the kth low frequency mode), the coupling can thus lead to temperature dependent shifts of optical transitions.

The absorption spectrum for the above model includes a zero phonon line (ZPL), consisting of contributions from all transitions for which the total number of phonons is unaltered upon excitation of the guest molecule. In addition, there is a phonon wing (PW), consisting of contributions for which the total number of phonons changes upon excitation of the guest molecule. The ZPL is a narrow Lorentzian, which loses intensity to the PW as the temperature is raised. For cyt *c*, the ZPL is only observed at temperatures below 50−60 K, in experiments where a small subpopulation of molecules is selectively excited such as in line-narrowed fluorescence spectroscopy.[67] In our conventional linear absorption experiments, inhomogeneous broadening prevents resolution of the ZPL.

In ref 35, the authors show that the absorption spectrum can be written as a sum of Voigtians, in which the Lorentzian components have a temperature dependent peak frequency. The temperature dependent shift of these peak frequencies is given by

$$\Delta(T) = \frac{N}{4}\left[\frac{\omega_{k,e}^2}{\omega_{k,g}^2} - 1\right]\hbar\langle\omega_k\rangle \coth(\hbar\langle\omega_k\rangle/2k_B T) \quad (7)$$

where N is the number of low frequency modes coupled to the electronic transition, and $\omega_{k,g}$ ($\omega_{k,e}$) is the effective phonon frequency when the molecule is in its ground (excited state). Equation 7 was obtained using an Einstein-like model for the phonon bath, where $\langle\omega_k\rangle$ is the average bath frequency. The ratio $R \equiv \omega_{k,e}^2/\omega_{k,g}^2$ is a measure of the quadratic electron−phonon coupling strength. Considering eq 7, the spectrum will shift to higher (lower) energies as the temperature is raised if the phonon frequencies in the excited electronic state are greater than (less than) the phonon frequencies in the electronic ground state. In other words, the spectrum will blue shift or red shift with increasing temperature if $R > 1$ or $R < 1$, respectively.

First consider temperatures for which $2k_B T \gg \hbar\langle\omega_k\rangle$, so that $\Delta(T) \approx N\ (R - 1)k_B T/2$. A red shift of the Q-band with increasing temperature is observed for all of the cytochromes studied here, as well as MP-11. If the principle contribution to this red-shift is given by coupling of the heme electronic transition to low frequency vibrations, then this shows $R < 1$. Therefore, the vibrational frequencies are decreased (the lattice force constants decrease) when the heme is excited. This of course neglects the contribution to the shift due to thermal expansion of the lattice. Below the glass transition temperature, the Q-band shifts by about $-0.167\ \text{cm}^{-1}$/K, which allows us to roughly estimate $N(R - 1) \approx -0.480$. The analysis of ref 35 showed that the temperature dependence of the B-band line width and shift of myoglobin and azurin are described well by the above model, using an average bath vibrational energy for the ground state of about 130−180 cm^{-1}, and coupling to $N = 50$ modes. Assuming the same number for cytochrome *c* yields $R = 0.990$.

We point out that at room temperature, where $k_BT = 207$ cm^{-1}, the spectral shifts of cyt *c* and MP-11 are more strongly temperature dependent than below the glass transition at about 180 K (where $k_BT = 125$ cm^{-1}). This has been attributed to anharmonic motions of the matrix.[35] The temperature dependence becomes almost negligible at temperatures below ~80 K (see Figures 2 and 3). At this temperature $k_BT = 56$ cm^{-1}, suggesting that the modes contributing to the temperature dependence have an average vibrational frequency given roughly by 56 cm^{-1} < $\hbar\langle\omega\rangle$ < 207 cm^{-1} (supporting the use of $\hbar\langle\omega\rangle \approx 130-180$ cm^{-1} above). This is because electron−phonon coupling will only lead to temperature dependent spectral shifts if the number of vibrational quanta in one or more phonon modes changes significantly over the temperature range considered. When k_BT is much less than the phonon energy of a given mode, this mode will remain unpopulated when the temperature is varied, and thus it will not contribute to the temperature dependence of the spectra.

It is important to note that cyt *c* and MP-11 approximately show the same temperature dependent shift. In fact, previous studies have shown that Zn coproporphyrin III in a glassy matrix and in a polyvinylchloride film shows a similar temperature dependent shift.[19] Thus the effect is somewhat insensitive to the immediate protein environment. These findings suggest that the temperature dependence involves either coupling to localized vibrations (such as the low frequency vibrations of the porphyrin ring itself), or to solvent phonons, or a combination of both. Possible candidates for localized modes that couple to the heme electronic transition are the low frequency out-of-plane vibrations of the porphyrin ring. Modes such as B_{2u} saddling (65 cm^{-1}), B_{1u} ruffling (88 cm^{-1}), A_{2u} doming (135 cm^{-1}), and E_g waving (176 cm^{-1}) fall within the frequency range calculated above, which could lead to the observed temperature dependence (frequency values obtained from ref 2)). For cyt *c* and MP-11, coupling to such out-of-plane porphyrin modes may also involve local protein motions, coupled either via the covalent cysteine linkages or the axial groups. While direct coupling of the porphyrin electronic transition to solvent modes is likely for Zn coproporphyrin III, and conceivable for MP-11, the coupling between the heme and the solvent in the case of cyt *c* is likely to be mediated by the protein. The above points will be discussed further in the following section.

VIII. Discussion and Conclusions

In this paper, our objective has been to present a systematic evaluation of the relative contributions of heme distortion and electrostatic interactions to the low-temperature splitting ΔQ_o observed for the Q(0,0) band of cyt *c*. ZINDO/S-SCI calculations demonstrated the possibility that heme distortions from D_{4h} symmetry can lead to a significant contribution to ΔQ_o, although the values of the calculated splittings were not consistent with the experimental trends. This may be a consequence of how the electronic energy levels vary with respect to the bond lengths and angles in the ZINDO/S method. Incorporation of the heme pocket electric field calculated using Poisson−Boltzmann electrostatics into a five-state model representing heme electronic states demonstrated that electrostatic interactions with the surrounding protein can also contribute significantly to ΔQ_o. Assuming a splitting due to heme distortion $\Delta Q_{Distortion} = 30$ cm^{-1}, the electrostatic interaction of the heme with the rest of the protein was shown to well reproduce the experimental values of ΔQ_o for HH, TH, and Y cyt *c*.

It is important to note that the large magnitude of the heme pocket internal field does not, by itself, reproduce the observed trend. This is because the interaction of a uniform field with a molecule is given by the scalar product of the dipole moment operator and the electric field vector. Since centrosymmetric molecules such as porphyrin have no permanent dipole moment in any eigenstate, the origin of the interaction is between the field and the transition dipole moments of the molecule. Because the Q(0,0) transition is relatively weak, with a transition dipole moment of only about 2-3 D, the large electric field magnitudes calculated and measured[10,11,15] for the cyt *c* heme pocket only contribute about 10 cm^{-1} to ΔQ_o. The main effect of the large field magnitude is to shift the transition energy due to interaction with the large Soret band transition dipole. This causes a significant shift in the ground state energy, and thus indirectly affects the Q-band transition energy.

Although the permanent dipole moment of the porphyrin ring is zero in any eigenstate, the permanent quadrupole moments are large. Our modeling suggests that the interaction of these quadrupole moments with the large internal field gradients calculated for HH, TH, and Y cyt *c* can lead to the observed trend in ΔQ_o. Interaction between the field gradients and the transition quadrupole moments also occurs, but the influence on ΔQ_o appears to be small (see Figure 10). However, more detailed calculations of the transition quadrupole moments need to be done in order to accurately assess this contribution. We are also currently studying the influence of the quadrupole terms on the spectra of other heme proteins.

We point out that the assumption of $\Delta Q_{Distortion} = 30$ cm^{-1} for HH, TH, and Y cyt *c* is not at all unrealistic. First, normal coordinate decomposition of out-of-plane heme distortions indicates that the character and magnitude of the distortion is conserved for these proteins.[1,2] This has been attributed to the fact that the amino acid sequence between the cys14* and cys17* residues, both covalently bound to the heme group via thioether linkages, is conserved for HH, TH, and Y(iso-1) cyt *c* (Y(iso-1) is the most abundant[68,69]). Although the heme distortions are significant, one could argue that the effects of out-of-plane distortion on ΔQ_o are unlikely to lead to large values of ΔQ_o on their own, since the largest displacements occur along normal coordinates for which the $x-y$ symmetry is not significantly disrupted.[70] The other smaller out-of-plane distortions combined with slight deviations in bond lengths are most likely to lead to a small value of $\Delta Q_{Distortion}$. Small variations in the distortion for HH, TH, and Y cyt *c* may result from hydrogen bonding between the heme propionates and different residues when comparing these proteins. However, these variations are more likely to lead to variations in the Q-band transition energy[8] than in the splitting, although this neglects the strong influence of the internal field. It is important to note that the strong internal field tends to blue-shift the Q(0,0) band, which is expected to compete with the tendency of the Q(0,0) band to red shift upon nonplanar distortion (due to destabilization of the ground state relative to the excited states). This might explain why the lowest transition energy ϵ_{Q_1} tends to vary so little from species to species.

Studies on Y cyt *c* mutants show that ΔQ_o can be increased by substituting the trp59 and ser40 residues.[30,31] For example, substituting trp59 with tyrosine increases ΔQ_o by about 10 cm^{-1}. This suggests that trp59 plays an important role in the Q-band splitting. However, trp59 is an evolutionary invariant residue, conserved for HH, TH, and Y cyt *c*, and yet there is still a large variation in ΔQ_o among these species. As discussed above, ΔQ_o contains contributions from both porphyrin ring distortion and from electrostatic interactions, and both vary to some extent among different cytochromes *c*. The crystal structures of HH,

TH, and Y cyt *c* all suggest possible hydrogen bonding between trp59 and one of the heme propionates, which may contribute significantly to ΔQ_o through direct distortion of the heme. Thus, it makes sense that replacement of this residue in the mutant structures might alter the heme conformation significantly. In addition, the neighboring amino acids differ for HH (val58-trp59-asn60), TH (thr58-trp59-lys60), and Y (leu58-trp59-asp60). Thus, it is possible that resulting variations in the secondary/tertiary structure in the vicinity of trp59 lead to slight variations in $\Delta Q_{\text{Distortion}}$. However, since the heme distortion is basically conserved for these proteins as discussed above, these variations are likely to be small. It is more likely that the variation in ΔQ_o for the cytochromes *c* studied here is due to the fact that the nonconserved residues differ in charge or polarity. Thus, when the polar asn60 in HH cyt *c* is replaced by the positively charged lys60 in TH cyt *c*, or by the negatively charged asp60 in Y cyt *c*, the electrostatic environment in the heme pocket is expected to vary. A similar effect is seen in the Y cyt *c* mutant studies: substitution of trp59 with tyrosine, which has a polar side chain at neutral pH, has a greater effect than substitution with phenylalanine or leucine, both of which have neutral, nonpolar side chain functional groups.

The Y cyt *c* mutant studies also showed that substitution of the ser40 residue with phenylalanine (with trp59 substituted by cysteine) increases ΔQ_o by about 15 cm^{-1}. Interestingly, the neighboring gly41 residue also appears to be hydrogen bonded to one of the heme propionates, so again it is possible that the mutation alters the heme conformation. However, the mutation also involves the replacement of a residue possessing a polar side chain, with one possessing a nonpolar side chain. Therefore, it is also possible that the mutation alters the electrostatic environment in the heme pocket. It is also interesting that the sequence his39-ser40-gly41 in Y cyt *c* is replaced by lys39-thr40-gly41 in both HH and TH cyt *c*, for which ΔQ_o is substantially larger. Since the residues neighboring gly41 are different for HH and TH cyt *c* than for Y cyt *c*, there may be a difference in structure leading to a difference in ΔQ_o, but is more likely that the difference is due to electrostatic factors. Since lys39 in HH and TH cyt *c* is likely to be charged at the experimental pH, this can significantly modify the electric field gradient in the heme pocket, resulting in an increase in the value of ΔQ_o relative to that of Y cyt *c*. This supports the idea that the splitting due to distortion is roughly conserved and that the main effect of mutations on the splitting comes from modifications to the electrostatic environment of the heme.

Deconvolution of the low-temperature absorption spectra of MP-11 indicates the possibility of Q(0,0) splitting, but it is likely that the greater motional freedom for MP-11 leads to the larger low-temperature band widths we observed (see Figure 3), obscuring any splitting that might exist. Essentially, as the solvent matrix freezes, it is expected that a greater number of subconformations will be frozen out, and thus there will be significant inhomogeneous broadening at low temperatures. We also mention that it has been suggested in resonance Raman and molecular dynamics studies that a sixth ligand to Fe in MP-11 is water.[59] Any axial ligand with a large permanent dipole moment might be expected to act together with the axial histidine to produce a large electric field gradient across the heme. However, even if this is the case, it is also likely that the orientation of the dipole is randomized compared to the axial methionine in cyt *c*. Therefore, this would only contribute further to the broadening, which would help to obscure any spectral splitting for MP-11.

Another goal of this Paper has been to gain insight into the origin of the temperature dependent spectral shift of the Q-band. Quadratic electron−phonon coupling can lead to the observed spectral shift as long as k_BT is on the order of the average phonon bath vibrational frequency or greater. The temperature dependent shift levels off at around 80 K for the proteins studied here. At this point $k_BT \sim 56$ cm^{-1}, which gives an estimate of the lower limit for the average bath vibrational frequency. We point out that cyt *c* and MP-11 show approximately the same temperature dependent shift. In addition, previous studies have shown that Zn coproporphyrin III in a glassy matrix and in a polyvinylchloride film shows a similar temperature dependent shift.[19] These findings suggest that the temperature dependence involves either coupling to the low-frequency vibrations of the porphyrin ring itself,[2] or to solvent phonons, or a combination of both.

For cyt *c* and MP-11, there may be additional contributions from localized protein motions, coupled either via the covalent cysteine linkages or the axial groups. This hypothesis is supported by the fact that Zn-cyt *c* shows an extremely weak temperature dependent shift compared to Zn coproporphyrin III and Fe cyt *c*.[19] For Zn cyt *c*, NMR measurements indicate that the axial his18† and met80† groups are in the same position as in Fe(II) cyt *c*,[71] and that the covalent linkages to the protein are the same. Therefore, the difference found in the temperature dependent Q-band shift when comparing Zn cyt *c* and Fe(II) cyt *c* is likely to be due to the way the metal couples to the axial ligands. In Zn−porphyrin coordination complexes, the metal is believed to be displaced out of the porphyrin plane towards an axial ligand.[72−74] It is thus possible that the porphyrin ring is stiffer with respect to out-of-plane motions due to the axial coordination in Zn cyt *c*. If this is the case, then Fe(II) cyt *c* probably shows a stronger temperature dependent Q-band shift because Fe is less stiff with respect to out-of-plane motions than Zn.

There are other possibilities to consider that could affect the temperature dependence of the Q(0,0) transition energy. First, it has been well established that hydrogen bonding strength exhibits temperature dependence.[75] However, FT−IR temperature profiling studies on α-helical proteins indicate that, in a glycerol−water matrix, the hydrogen bonds that maintain the secondary structure are very weakly temperature dependent from room temperature to 10 K.[76] Since the average hydrogen bond angles are not expected to fluctuate as much for a well defined protein secondary structure (such as the hydrogen bonds holding an α-helix together) as for solvated groups with little or no structure, the insensitivity of hydrogen bonding strength to temperature is understandable. Thus, we find it unlikely that interresidue hydrogen bonding, or the hydrogen bonding between the heme group and the protein residues, exhibits a strong enough temperature dependence to lead to the observed spectral shifts for cyt *c*. The greater solvent exposure of the heme group in MP-11 does suggest the possibility that hydrogen bonding might play a role in the temperature shift of the Q-band. However, it is unclear how this would lead to such a prominent shift in this protein, or how this would explain the sensitivity of the temperature dependence to the central metal ion of the porphyrin ring.

There also exists the possibility that thermal contraction of the lattice contributes to the temperature dependence of the Q-band. It has been shown that this effect acts together with quadratic electron−phonon coupling to produce ZPL temperature shifts in impurity crystals.[77−80] The mechanism in the case of impurity crystals was a displacement of the electronic potential energy of the impurity levels due to thermal expansion/

contraction. In our case, this could represent an increase in out-of−plane distortion of the heme as the temperature is lowered, due to lattice contraction. However, such a distortion is expected to red shift the Q-band, whereas we see a blue shift of the Q-band as the temperature is lowered. It is possible that the distortion induced red shift competes with the electron−phonon coupling induced blue shift as the temperature is lowered, leading to the weak temperature dependence of the transition energies ϵ_{Q_1} and ϵ_{Q_2} below 80 K.

We can also consider the possibility that the axial ligands become more strongly bound as the temperature is lowered. This might cause the Q-band to blue shift as the temperature is lowered. However, if the Fe-His18† or Fe-Met80† distances changed enough with temperature to lead to the observed blue-shift, then the splitting would be expected to increase as well. On the contrary, we find that the Q(0,0) splitting, once resolved, is approximately independent of temperature. Since the splitting is relatively insensitive to temperature, we feel that this effect plays a smaller role in the temperature dependence of the Q-band energy.

At higher temperatures (above the solvent glass transition), when ΔQ_o is unresolved, it is likely that thermal motions lead to variations in both ΔQ_o and ϵ_{Q_1}. Poisson−Boltzmann electrostatics calculations along different points of a molecular dynamics trajectory for cyt *c* do indicate that the internal field, as well as the heme conformation, fluctuates in time.[81] Thus it is possible that the average field in the heme pocket is lower and the out-of-plane distortion is greater, leading to a red-shift with increasing temperature. Such electric field fluctuations are consistent with an increase in the Q_1- and Q_2-band line widths, providing an explanation for why ΔQ_o is unresolved at room temperature. However, more studies will need to be done in order to quantify the influence of internal field fluctuations on the Q-band splitting and temperature shift.

Acknowledgment. This work was supported by the National Institute of Health Grants PO1 GM48310 and R01 GM55004. We also gratefully acknowledge Professor Michael C. Zerner and Professor John A. Shelnutt for very helpful discussions. We thank Professor Shelnutt for kindly supplying normal coordinate structural decomposition data for the hemes.

References and Notes

(1) Hobbs, J. D.; Shelnutt, J. A. *J. Protein Chem.* **1995**, *14*, 19.
(2) Jentzen, W.; Ma, J.-G.; Shelnutt, J. A. *Biophys. J.* **1998**, *74*, 753.
(3) Barkigia, K. M.; Renner, M. W.; Furenlid, L. R.; Medforth, C. J.; Smith, K. M.; Fajer, J. *J. Am. Chem. Soc.* **1993**, *115*, 3627.
(4) Ma, J.-G.; Laberge, M.; Song, Z.-Z.; Jentzen, W.; Jia, S.-L.; Vanderkooi, J. M.; Shelnutt, J. A. *Biochemistry* **1997**, *37*, 5118.
(5) Ma, J.-G.; Jentzen, W.; Laberge, M.; Vanderkooi, J.; Song, X.-Z.; Jia, S.-L.; Hobbs, J. D.; Shelnutt, J. *Biophys. J.* **1997**, *72*, A10.
(6) Shelnutt, J. A.; Rousseau, D. L.; Dethmers, J. K.; Margoliash, E. *Biochemistry* **1981**, *20*, 6485.
(7) Shelnutt, J. A.; Rousseau, D. L.; Dethmers, J. K.; Margoliash, E. *Proc. Natl. Acad. Sci. U.S.A.* **1979**, *76*, 3865.
(8) Jentzen, W.; Simpson, M. C.; Hobbs, J. D.; Song, X.; Ema, T.; Nelson, N. Y.; Medforth, C. J.; Smith, K. M.; Veyrat, M.; Mazzanti, M.; Ramasseul, R.; Marchon, J.-C.; Takeuchi, T.; Goddard, W. A. I.; Shelnutt, J. A. *J. Am. Chem. Soc.* **1995**, *117*, 11085.
(9) Anni, H.; Vanderkooi, J. M.; Sharp, K. A.; Yonetani, T.; Hopkins, S. C.; Herenyi, L.; Fidy, J. *Biochemistry* **1994**, *33*, 3475.
(10) Geissinger, P.; Kohler, B. E.; Woehl, J. C. *J. Phys. Chem.* **1995**, *99*, 16527.
(11) Geissinger, P.; Kohler, B. E.; Woehl, J. C. *Synth. Met.* **1997**, *84*, 937.
(12) Laberge, M.; Sharp, K. A.; Vanderkooi, J. M. *Biophys. Chem.* **1998**, *71*, 9.
(13) Laberge, M.; Sharp, K. A.; Vanderkooi, J. M. *J. Phys. Chem.* **1997**, *101*, 7364.
(14) Laberge, M.; Vanderkooi, J. M.; Sharp, K. A. *J. Phys. Chem.* **1996**, *100*, 10793.
(15) Köhler, M.; Gafert, J.; Friedrich, J.; Vanderkooi, J. M.; Laberge, M. *Biophys. J.* **1996**, *71*, 77.
(16) Honig, B.; Nicholls, A. *Science* **1995**, *268*, 1144.
(17) Lockhart, D. M.; Kim, P. S. *Science* **1992**, *257*, 947.
(18) Gouterman, M. *The Porphyrins*; Dolphin, D., Ed; Academic Press: New York, 1978; Vol. III, pp 1−156.
(19) Reddy, K. S.; Angiolillo, P. J.; Wright, W. W.; Laberge, M.; Vanderkooi, J. M. *Biochemistry* **1996**, *35*, 12820.
(20) Balog, E.; Kis-Petik, K.; Fidy, J.; Kohler, M.; Friedrich, J. *Biophys. J.* **1997**, *73*, 397.
(21) Wagner, G. C.; Kassner, R. J. *Biochem. Biophys. Res. Commun.* **1975**, *63*, 385.
(22) Keilin, D.; Hartree, E. F. *Nature* **1949**, *164*, 254.
(23) Friedman, J. M.; Rousseau, D. L.; Adar, F. *Proc. Natl. Acad. Sci. U.S.A.* **1977**, *74*, 2607.
(24) Wilson, D. F. *Arch. Biochem. Biophys.* **1967**, *121*, 757.
(25) Ahn, J. S.; Kitagawa, T.; Kanematsu, Y.; Nishikawa, Y.; Kushida, T. *J. Lumin.* **1995**, *64*, 81.
(26) Champion, P. M.; Collins, D. W.; Fitchen, D. B. *J. Am. Chem. Soc.* **1976**, *98*, 7114.
(27) Hagihara, B.; Oshino, R.; Iizuka, T. *J. Biochem.* **1974**, *75*, 45.
(28) Cowan, J. A.; Gray, H. B. *Inorg. Chem.* **1989**, *28*, 4554.
(29) Shelnutt, J. A. *J. Chem. Phys.* **1980**, *72*, 3948.
(30) Schweingruber, M. E.; Sherman, F.; Stewart, J. W. *J. Biol. Chem.* **1977**, *252*, 6577.
(31) Schweingruber, M. E.; Stewart, J. W.; Sherman, F. *J. Biol. Chem.* **1979**, *254*, 4132.
(32) Gradl, G.; Kohler, B. E.; Westerfeld, J. *Chem. Phys.* **1992**, *97* , 6064.
(33) Kohler, B. E.; Woehl, J. C. *J. Chem. Phys.* **1995**, *102*, 7773.
(34) Eaton, W. E.; Hochstrasser, R. M. *J. Chem. Phys.* **1967**, *46*, 2533.
(35) Cupane, A.; Leone, M.; Vitrano, E.; L., C. *Eur. Biophys. J.* **1995**, *23*, 385.
(36) Cordone, L.; Cupane, A.; Leone, M.; Vitrano, E. *Biophys. Chem.* **1986**, *24*, 259.
(37) Di Pace, A.; Cupane, A.; Leone, M.; Vitrano, E.; Cordone, L. *Biophys. J.* **1992**, *63*, 475.
(38) Urry, D. W. *J. Am. Chem. Soc.* **1967**, *89*, 4190.
(39) Harbury, H. A.; Loach, P. A. *J. Biol. Chem.* **1960**, *235*, 3640.
(40) Bacon, A. D.; Zerner, M. C. *Theor. Chim. Acta* **1979**, *53*, 21.
(41) Ridley, J.; Zerner, M. C. *Theor. Chim. Acta* **1973**, *32*, 111.
(42) Ridley, J. E.; Zerner, M. C. *Theor. Chim. Acta* **1976**, *42*, 223.
(43) Frisch, M. J.; Trucks, G. W.; Schlegel, H. B.; Gill, P. M. W.; Johnson, B. G.; Robb, M. A.; Cheeseman, J. R.; Keith, T.; Petersson, G. A.; Montgomery, J. A.; Raghavachari, K.; Al-Laham, M. A.; Zakrzewski, V. G.; Ortiz, J. V.; Foresman, J. B.; Cioslowski, J.; Stefanov, B. B.; Nanayakkara, A.; Challacombe, M.; Peng, C. Y.; Ayala, P. Y.; Chen, W.; Wong, M. W.; Andres, J. L.; Repogle, E. S.; Gomperts, R.; Martin, R. L.; Fox, D. J.; Binkley, J. S.; Defrees, D. J.; Baker, J.; Stewart, J. P.; Head-Gordon, M.; Gonzalez, C.; Pople, J. A. *Gaussian 94*, Revision E.2; Pittsburgh PA, 1995.
(44) Makinen, M. W.; Churg, A. K. *Iron Porphyrins*; Lever, A. B. P., Gray, H. B., Ed; Addison-Wesley: Reading, MA, 1983; Vol. 1, pp 141−235.
(45) Edwards, W. D.; Weiner, B.; Zerner, M. C. *J. Am. Chem. Soc.* **1986**, *108*, 1309.
(46) Du, P.; Axe, U.; Loew, G. H.; Canuto, S.; Zerner, M. C. *J. Am. Chem. Soc.* **1991**, *113*, 8614.
(47) Nicholls, A.; Honig, B. *J. Comp. Chem.* **1991**, *12*, 435.
(48) Jayaram, B.; Sharp, K. A.; Honig, B. *Biopolymers* **1989**, *28*, 975.
(49) Gilson, M.; Sharp, K.; Honig, B. *J. Comp. Chem.* **1988**, *9*, 327.
(50) Sharp, K.; Honig, B. *Ann. Rev. Biophys. Chem.* **1990**, *19*, 301.
(51) Nicholls, A.; Sharp, K. A.; Honig, B. *Proteins* **1991**, *11*, 281.
(52) Sitkoff, D.; Sharp, K. A.; Honig, B. *J. Phys. Chem.* **1994**, *98*, 1978.
(53) Bushnell, G. W.; Louie, G. V.; Brayer, G. D. *J. Mol. Biol.* **1990**, *214*, 585.
(54) Takano, T.; Dickerson, R. E. *J. Mol. Biol.* **1981**, *153*, 79, 95−115.
(55) Louie, G. V.; Brayer, G. D. *J. Mol. Biol.* **1990**, *214*, 527.
(56) Thompson, M. A.; Zerner, M. C. *J. Am. Chem. Soc.* **1991**, *113*, 8210.
(57) Karelson, M. M.; Zerner, M. C. *J. Phys. Chem.* **1992**, *96*, 6949.
(58) Broo, A.; Pearl, G.; Zerner, M. C. *J. Phys. Chem. A.* **1997**, *101*, 2478.
(59) Laberge, M.; Vreugdenhil, A. J.; Vanderkooi, J. M.; Butler, I. S. *J. Biomol. Struct. Dyn.* **1998**, *15*, 1039.
(60) Angiolillo, P.; Vanderkooi, J. M. *Biophys. J.* **1995**, *68*, 2505.
(61) Spiro, T. G.; Strekas, T. C. *Proc. Natl. Acad. Sci. U.S.A.* **1972**, *69*, 2622.
(62) Valance, W. G.; Strekas, T. C. *J. Phys. Chem.* **1982**, *86*, 1804.

(63) Shelnutt, J. A.; Cheung, L. D.; Chang, R. C. C.; Yu, N.-T.; Felton, R. H. *J. Chem. Phys.* **1977**, *66*, 3387.

(64) Laberge, M.; Wright, W. W. 1997. Unpublished work.

(65) The PARSE charges are (0.155, −0.560, 0.155) for the CE1-NE1-CE2 dipole of his18† and (0.265, −0.530, 0.265) for the CE-SD-CG dipole of met80†.

(66) Bottcher, C. J. F. *Theory of Electric Polarization*; Elsevier Press: Amsterdam, 1973.

(67) Vanderkooi, J. M.; Angiolillo, P. J.; Laberge, M. *Methods Enzymol.* **1997**, *278*, 71.

(68) Sels, A. A.; Fukuhara, G.; Pere, G.; Slonimski, P. P. *Biochim. Biophys. Acta* **1965**, *95*, 486.

(69) Sherman, F.; Stewart, J. W. *Biochemistry and Genetics of Yeast*; Bacila, M., Horecker, B. L., Stoppani, A. O. M., Ed; Academic Press: New York, 1978; pp 273−316.

(70) Shelnutt, J. A. Personal Communication.

(71) Anni, H.; Vanderkooi, J. M.; Mayne, L. *Biochemistry* **1995**, *34*, 5744.

(72) Scheidt, W. R.; Eigenbrot, C. W.; Ogiso, M.; Hatano, K. *Bull. Chem. Soc. Jpn* **1987**, *60*, 3529.

(73) Scheidt, W. R.; Mondal, J. U.; Eigenbrot, C. W.; Adler, A.; Radonovich, L. J.; Hoard, J. L. *Inorg. Chem.* **1986**, *25*, 795.

(74) Schauer, C. K.; Anderson, O. P.; Eaton, S. S.; Eaton, G. R. *Inorg. Chem.* **1985**, *24*, 4082.

(75) Jeffrey, G. A. *An Introduction to Hydrogen Bonding*; Oxford University Press: New York, 1997.

(76) Manas, E. S.; Vanderkooi, J. M.; Wright, W. W. 1999. Unpublished work.

(77) Personov, R. I. *Spectroscopy and Excitation Dynamics of Condensed Molecular Systems*; Agranovich, V. M., Hochstrasser, R. M., Ed.; North-Holland Publishing Co.: Amsterdam, 1983; pp 555−619.

(78) Osad'ko, I. S. *Spectroscopy and Excitation Dynamics of Condensed Molecular Systems*; Agranovich, V. M., Hochstrasser, R. M., Ed.; North-Holland Publishing Co.: Amsterdam, 1983; pp 437−514.

(79) Burns, M. J.; Liu, W. K.; Zewail, A. H. *Spectroscopy and Excitation Dynamics of Condensed Molecular Systems*; Agranovich, V. M., Hochstrasser, R. M., Ed.; North-Holland Publishing Co.: Amsterdam, 1983; pp 301−435.

(80) Stoneham, A. M. *Theory of Defects in Solids: Electronic Structure of Defects in Insulators and Semiconductors*; Oxford University Press: New York, 1975.

(81) Laberge, M.; Köhler, M.; Vanderkooi, J. M.; Friedrich, J. *Biophys. J.*, **1999**. Submitted for publication.